Non-unit Protection Scheme Based on Cooperation with Control Strategy for Multiterminal Hybrid HVDC System Without Line Boundary

Ye Li, Na Jia, Jiawei He, Bin Li, *Member*, *IEEE*, Haiyang Wang, and Shengbo Zhang

***Abstract*—Multiterminal hybrid HVDC systems, combining the advantages of conventional and flexible DC systems, are considered important development trends for future power networks. With the ability to suppress DC fault current, hybrid HVDC systems eliminate the requirement of current limiting reactors at both ends of DC lines. Thus, non-unit protection based on line boundaries is no longer applicable. In this paper, a non-unit protection scheme in cooperation with converter control is proposed to ensure protection speed, reliability, and sensitivity for multiterminal hybrid HVDC systems without line boundaries. In the proposed protection scheme, the protection criterion based on the transient energy of the DC voltage and the direction criterion based on the travelling wave are used to identify whether the fault occurs on the DC line. When the fault is detected as a DC-line fault, the relevant converter station is quickly blocked. After a specified hold-off duration, the converter station interfacing with multiple DC lines is prioritized for restart, while the remaining converter stations are restarted once the DC voltage is stabilized. Simulations based on PSCAD/EMTDC validate the feasibility of the proposed protection scheme and its superiority over competing approaches.**

***Index Terms*—Multiterminal hybrid HVDC system, non-unit protection scheme based on cooperation with control strategy, independent of line boundary.**

Received: October 18, 2024
Accepted: April 28, 2025
Published Online: September 1, 2025

Ye Li, Na Jia, Haiyang Wang, and Shengbo Zhang are with the State Key Laboratory of Intelligent Power Distribution Equipment and System, the School of Electrical Engineering, Hebei University of Technology, Tianjin 300401, China (e-mail: liye@hebut.edu.cn; 202221401115@stu.hebut.edu.cn; 202321401039@stu.hebut.edu.cn; 202321401077@stu.hebut.edu.cn).

Jiawei He (corresponding author) and Bin Li are with the State Key Laboratory of Intelligent Power Distribution Equipment and System, the School of Electrical and Information, Tianjin University, Tianjin 300072, China (e-mail: hejiawei_tju@126.cn; binli@tju.edu.cn).

DOI: 10.23919/PCMP.2024.000190

I. Introduction

Accelerating the utilization of renewable energy and building an interconnected global energy infrastructure are necessary to promote energy revolution and realize the broad utilization of clean energy [1], [2]. Large-scale renewable energy sources are often located far from load center, and thus require long-distance, high-capacity energy transmission, leading to the development and utilization of DC transmission technology [3]. As line-commutated converter (LCC) inverter stations suffer from the risk of commutation failure, conventional HVDC transmission systems based on LCC are generally used for point-to-point systems [4], [5]. Multiterminal hybrid HVDC systems combining the advantages of conventional and flexible DC transmission technologies, have promising development prospects. Rectifier stations, which are based on LCC, saves investments, and inverter stations, which are based on modular multilevel converter (MMC), enhance the operation flexibility of such networks [6]. This system retains the large transmission capacity of conventional DC transmission technology and uses a flexible DC converter to provide voltage support, avoiding the risk of LCC-based converter commutation failure problems [7].

At present, planned and constructed multiterminal hybrid HVDC systems mainly use high-voltage DC overhead lines, which greatly increases the risk of DC line faults [8], [9]. Therefore, rapid DC fault isolation is a key technology for improving real-world application prospects of multiterminal hybrid HVDC system. DC fault isolation method is greatly affected by the topology of the multiterminal hybrid HVDC system. The combination of a half bridge submodule (HBSM) based MMC and a DC circuit breaker, and the combination of a fault self-clearing converter and a DC disconnector are typical structures used to isolate DC faults [10], [11]. The differences in these topologies lead to marked differences in identifying and isolating DC faults, necessitating research into DC fault protection principles for different HVDC systems.

For a flexible HVDC system constructed with HBSM-based MMC and DC circuit breaker, installing current limiting inductors is necessary to limit the rapid rise of fault current, and these inductors cooperate with

the DC circuit breaker to isolate the fault [12], [13]. Many researchers have proposed non-unit protection schemes that utilize the blocking effect of boundary elements.

The voltage change rate at the line side of the DC inductor is used to identify the fault location in [14] and [15]. Reference [16] analyzes the characteristics of the transmitted and reflected traveling wave (TW) at the line terminal and proposes a non-unit protection scheme that includes the fault section discrimination criterion based on the magnitude and change rate of the voltage, and the direction protection criterion based on the current change rate. Reference [17] introduces non-unit protection based on the reflected TW. Furthermore, to improve the ability of the protection to withstand transition resistance, reference [18] utilizes the transient voltage ratio at both sides of the current-limiting inductor to discriminate the fault section. Reference [19] analyzes the characteristic difference of internal and external faults considering the distribution and frequency variation characteristics of line parameters. Considering these prior works, a new non-unit protection based on the transient voltage energy is developed in this study.

An HVDC system based on a converter with fault isolation capability is another typical application scenario [20]. An example of such a HVDC system is the Wudongde hybrid HVDC grid in China, as shown in Fig. 1 [6]. In Fig. 1, inverter stations S_1 and S_2 are based on MMC composed of full bridge submodules (FBSMs) and HBSMs, and rectifier station S_3 is based on LCC. Because the MMC converters are composed of FBSMs and HBSMs, DC fault current limitation and clearance can be realized as the FBSMs can output reverse voltages. For the LCC-based station, when a DC fault occurs, the DC fault current can be limited and suppressed quickly by interrupting the thyristor trigger signal and controlling the phase shift. Since the converters can limit and restrain the fault current, the necessity of having a DC inductor installed at both DC line ends is greatly reduced.

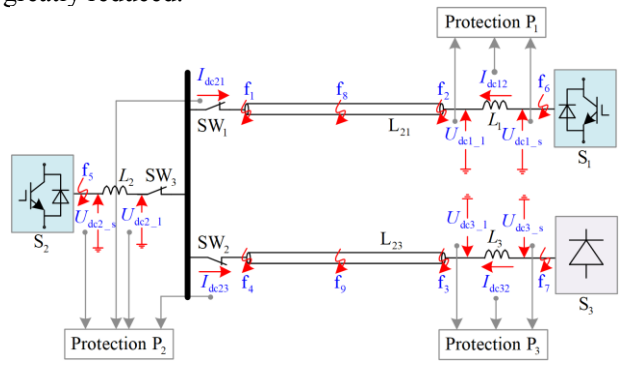

Fig. 1. The typical topology of the multiterminal hybrid HVDC system.

For this typical scenario, non-unit protection criteria based on the line boundary are not applicable because they cannot distinguish between a terminal fault on the protected line and an outlet fault of the adjacent line. For example, protection P_1 and P_3 cannot identify the fault f_1 and f_4 only based on the local traveling wave. Therefore, reference [21] proposes an active-signal-injection-based fault identification scheme, which relies on the control strategy to inject harmonic signals to the system. However, this method somewhat increases the complexity of converter control. Communication-based protection using two terminal quantities is another preferred solution. Related examples include direction pilot protection based on TW and current differential protection [22]–[25]. However, the delay caused by line communication severely affects the operation speed of the protection.

Therefore, this study designs a non-unit protection scheme based on cooperation with the control strategy for a hybrid multi-terminal direct current (MTDC) power grid without a line boundary. This scheme relies on only local information and can achieve rapid fault identification and recovery.

The rest content of this paper is as follows. Firstly, the performances of the existing protection criteria are compared, and the protection configuration for DC line fault identification in a multiterminal hybrid HVDC are provided in Section II. On this basis, in Section III, a non-unit protection scheme based on cooperation with control is proposed for the multiterminal hybrid HVDC system without a line boundary. The proposed scheme realizes rapid fault identification and recovery since it is based on single terminal electrical quantities. And then, the superiority of the proposed non-unit protection scheme over competing approaches is verified using the PSCAD/EMTDC simulation platform in Section IV. Finally, the conclusion is presented in Section V.

II. Protection Performances Analysis and Protection Configuration for DC Line Fault Identification in the Multiterminal Hybrid HVDC System

For the multiterminal hybrid HVDC system without line boundary shown in Fig. 1, it is not possible to accurately identify which line is the fault line. However, through the combination of the non-unit fault identification criteria and direction criteria, fast and reliable identification of the DC line fault can still be achieved. Therefore, the performances of the existing protection criteria are compared. On this basis, an appropriate setting calculation principle is developed.

A. Non-unit Protection Criteria for Fault Section Identification

To evaluate the performance of different non-unit protection criteria for fault section identification and

calculate the protection setting value, protection P_1 in Fig. 1 is taken as an example to analyze the characteristics of the DC fault at different positions. The main parameters of the system and line are listed in Table I and Table II, respectively.

TABLE I
HYBRID HVDC GRID PARAMETERS

Parameter	S_1	S_2	S_3
Rated AC voltage (kV)	525	525	535
Rated DC voltage (kV)	±780	±770	±800
DC inductor (mH)	75	75	150
Rated power (MVA)	5100	3132	9720
Arm inductor (mH)	41.2	61.2	
Submodule capacitance (μF)	18 000	12 000	
Submodule number	210	210	

TABLE II
HVDC LINE PARAMETERS

	Parameter	L_{21}	L_{23}
Ground wire	Hight (m)	72	64
	Horizontal spacing (m)	28	22
	Outer radius (mm)	15.75	15.75
	Sag (m)	15	13
	DC resistance (Ω/km)	0.5807	0.5807
Conductor	Hight (m)	64	58
	Horizontal spacing (m)	23	20
	Outer radius (mm)	36.23	47.35
	Sag (m)	26	18
	Length (km)	557	932
	DC resistance (Ω/km)	0.0391	0.022 91

For protection P_1, when an internal fault occurs, the time-domain voltage at protection P_1 can be obtained through Laplace transform, as shown in [26]. Therefore, the voltage variation, change rate of the voltage, and transient voltage energy of the different fault positions and fault transition resistances can be calculated, as shown in Figs. 2(a), (b) and (c), respectively. It should be noted that the transient component of the DC voltage is extracted by the wavelet transform, and according to the wavelet transform theory, the squared wavelet coefficients denote the energy of the signal within the corresponding frequency band, as illustrated in [27] and [28]. Therefore, when the wavelet transform is applied to the voltage, the square of the maximum detail coefficient represents the transient voltage energy.

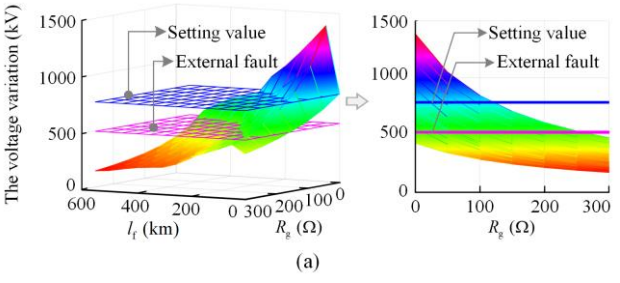

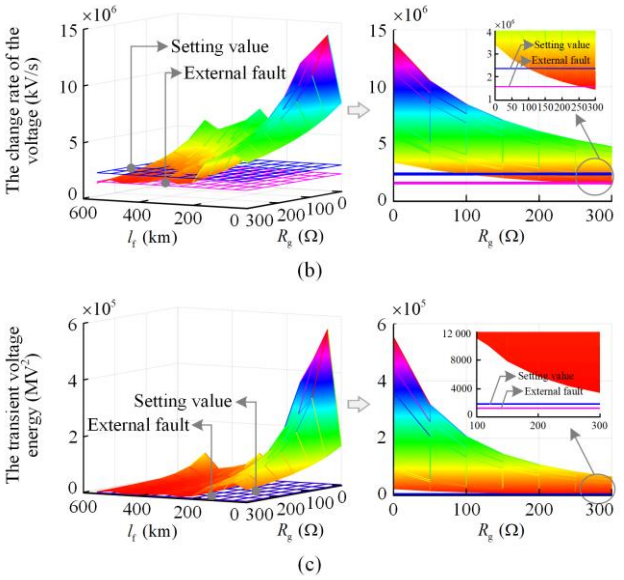

Fig. 2. Performance of the non-unit protection criteria for different fault positions and different fault transition resistances. (a) The voltage variation. (b) The change rate of the voltage. (c) The transient voltage energy.

As shown in Figs. 2(a) and (b), for a long-distance fault with a high transition resistance, the variation and change rate of the voltage are smaller than those of an external metallic fault, indicating that the non-unit protection criterion based on the time domain voltage has a weak tolerance to the transition resistance. However, compared with time-domain voltage-based non-unit protection criteria, the non-unit protection criterion based on transient voltage offers improved tolerance to fault resistance. This occurs due to the transient voltage of the internal remote fault with high transition resistance being larger than that of the external fault, as shown in Fig. 2(c). Therefore, the non-unit protection criterion based on the transient energy [19] is used, as shown:

$$\begin{cases} \text{internal fault: } E_{\mathrm{U}} = \left(\max\left|U_{\mathrm{t}}(k)\right|\right)^2 > E_{\mathrm{s}} \\ \text{external fault: } E_{\mathrm{U}} = \left(\max\left|U_{\mathrm{t}}(k)\right|\right)^2 \leqslant E_{\mathrm{s}} \end{cases} \tag{1}$$

where U_{t} is the DC transient voltage extracted by the wavelet algorithm; E_{s} is the protection setting value; and k represents the sampling point. For protection P_1, to ensure quick and sensitive action after DC-line faults and reliable no-action after non-DC-line faults, the setting value should be calculated as:

$$E_{\mathrm{s\_1}} = K_{\mathrm{r}} \max\left(E_{\mathrm{U\_f5}}, E_{\mathrm{U\_f7}}\right) \tag{2}$$

where K_{r} is the reliability coefficient of the protection criterion $\left(K_{\mathrm{r}} = 1.5\right)$; while $E_{\mathrm{U\_f5}}$ and $E_{\mathrm{U\_f7}}$ are the transient voltage energies at the line side of the DC inductor after metallic faults f_5 and f_7, respectively.

The proposed calculation method for the setting value of protection P_3 is similar to that of protection P_1.

However, for protections P_1 and P_3, the selectivity of the non-unit protection criterion cannot be guaranteed by only setting the protection value. For example, for protection P_1 installed at the outlet of station S_1, the magnitude of fault TW after DC fault f_1 is equal to that of fault TW after DC fault f_4, where f_1 is located at the end of L_{21} and f_4 is located at the beginning of L_{23}. Therefore, further research on a non-unit protection scheme that is independent of the line boundary is necessary for a multi-terminal hybrid HVDC grid, as discussed in section III.

However, for protection P_2, the fault occurring on the L_{21} side or L_{23} side can be identified by the direction protection criterion (which is introduced in section II.B). Therefore, it is necessary to further determine whether the fault occurs on the DC line using the transient-voltage-energy-based protection criterion. The corresponding setting value can be calculated as:

$$\begin{cases} E_{s\_2\_L21} = K_r E_{U\_f_6} \\ E_{s\_2\_L23} = K_r E_{U\_f_7} \end{cases} \tag{3}$$

where E_{U_f6} and E_{U_f7} are the DC transient voltage energies at the line side of the DC inductor at the outlet of station S_2 after metallic faults f_6 and f_7, respectively, as shown in Fig. 1.

B. The Protection Criteria for Fault Direction Identification

1) The Direction Criterion Based on the DC Transient Voltages at Both Sides of the DC Inductor

For situations where there is only one line connected to the converter, such as protections P_1 and P_3 in Fig. 1, the amplitude ratio of the high-frequency transient voltages at both sides of the DC inductor can be used to discriminate the fault direction, based on the attenuation effect of the DC inductor on high-frequency fault components. Thus, the direction criterion based on the magnitude ratio of the line-side DC transient voltage and converter-side transient voltage can be expressed as:

$$\begin{cases} \text{line-side fault}: K_d = \dfrac{\max\left|U_{l\_t}(k)\right|}{\max\left|U_{s\_t}(k)\right|} > K_{s1} \\ \text{converter-side fault}: K_d = \dfrac{\max\left|U_{l\_t}(k)\right|}{\max\left|U_{s\_t}(k)\right|} \leqslant K_{s1} \end{cases} \tag{4}$$

where U_{l_t} and U_{s_t} are the transient voltages of the line side and converter side of the DC inductor, respectively, which can be calculated using the wavelet algorithm; and K_{s1} denotes the setting value of the direction criterion, which is set to 1.1.

For a multi-terminal hybrid HVDC system with fault self-clearing capability, the DC inductor can be installed at the converter outlet, instead of each end of the DC line, as inductor L_2 shown in Fig. 1. Therefore, for the situation where there are multiple DC lines at the converter outlet (e.g., as protection P_2 in Fig. 1), the direction criterion based on the magnitude ratio of the transient voltage at both sides of the DC inductor can only identify whether the fault occurs on the DC line-side, while this criterion cannot distinguish whether the fault occurs on L_{21} side or L_{23} side. Therefore, a direction criterion that is independent of the line boundary is necessary.

2) The Direction Criterion Based on the Magnitude Ratio of the Forward and Reverse TWs

According to the analysis of the TW propagation characteristics, when a forward fault occurs, the amplitude ratio of the forward and reverse TWs is equal to the reflection coefficient within a specified time, while the amplitude ratio after the reverse fault is infinite. Therefore, the direction protection criterion based on the magnitude ratio of the forward and reverse TWs can be utilized to further identify the fault line direction, which is independent of the line boundary, shown as:

$$\begin{cases} \text{forward fault}: K_{SW} < K_{s2} \\ \text{reverse fault}: K_{SW} \geqslant K_{s2} \end{cases} \tag{5}$$

where K_{SW} is the magnitude ratio of the forward and reverse TWs; and K_{s2} is the setting value of the direction protection criterion based on the TW, which is affected by the reflection coefficient. It should be noted that the calculation of the reflection coefficient is based on the converter. Because the time window of the direction criterion based on TWs is tiny, the fault response of the converter need not be considered. Therefore, the reflection coefficient can be obtained by the equivalent impedance of the converter with normal operation, which is usually less than 1. For K_{s2}, it is set to 1.5.

Therefore, for the direction protection criterion based on the magnitude ratio of the forward and reverse TWs, it is very important to accurately extract the forward and reverse TWs. To eliminate the coupling effect of the positive and negative poles of the DC line, the line mode components of the DC voltage and current are utilized to identify the fault in this paper. Therefore, based on [24], the line-mode fault voltage TW and current TW can be calculated as:

$$\begin{cases} \Delta U(f) = F(f)\mathrm{e}^{-\gamma(f)x} + B(f)\mathrm{e}^{\gamma(f)x} = \Delta U_F(f) + \Delta U_B(f) \\ \Delta I(f) = \dfrac{F(f)}{Z_c(f)}\mathrm{e}^{-\gamma(f)x} - \dfrac{B(f)}{Z_c(f)}\mathrm{e}^{\gamma(f)x} = \dfrac{\Delta U_F(f)}{Z_c(f)} - \dfrac{\Delta U_B(f)}{Z_c(f)} \end{cases} \tag{6}$$

where f denotes the frequency; $F(f)$ and $B(f)$ are

the amplitude of the forward and reverse fault voltage TWs respectively; $\gamma(f)$ is the propagation; $Z_c(f)$ is the wave impedance; $\Delta U_F(f)$ and $\Delta U_B(f)$ represent the respective forward and reverse fault voltage TWs, which can be calculated as:

$$\begin{cases} \Delta U_F(f) = \dfrac{\Delta U(f) + \Delta I(f) Z_c(f)}{2} \\ \Delta U_B(f) = \dfrac{\Delta U(f) - \Delta I(f) Z_c(f)}{2} \end{cases} \tag{7}$$

Based on [29], neither the fault voltage nor the current contains low-frequency components during the initial stage of the fault. In addition, the line-mode wave impedance corresponding to the high frequency is a fixed value, as shown in Fig. 3. For example, within the high frequency band, the line-mode wave impedance of L_{21} is $Z_{c\_L21} = 240\ \Omega$, while the line-mode wave impedance of L_{23} is $Z_{c\_L23} = 220\ \Omega$. Therefore, when the DC voltage variation, DC current variation, and high-frequency wave impedance are utilized, the forward and reverse TWs can be obtained accurately. This indicates that, the forward fault TWs for protection P_2 can be accurately calculated by $\Delta U_{dc2\_1} + \Delta I_{dc21} Z_{c\_L21}$ and $\Delta U_{dc2\_1} + \Delta I_{dc23} Z_{c\_L23}$, while the reverse fault TWs can be accurately calculated by $\Delta U_{dc2\_1} - \Delta I_{dc21} Z_{c\_L21}$ and $\Delta U_{dc2\_1} - \Delta I_{dc23} Z_{c\_L23}$.

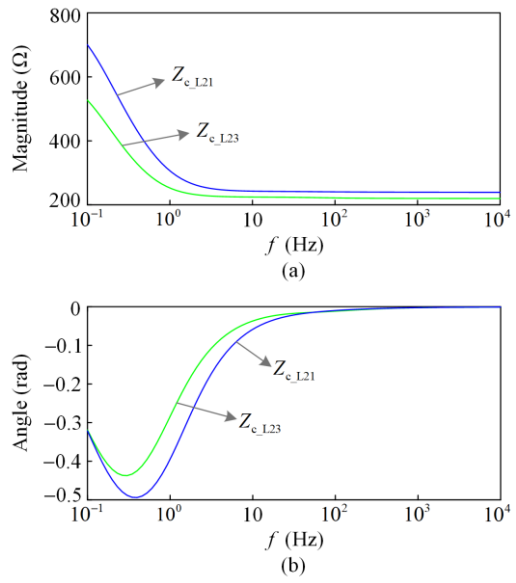

Fig. 3. The magnitude and angle of the wave impedance. (a) The magnitude of the wave impedance. (b) The angle of the wave impedance.

Therefore, and the magnitude ratio of the forward and reverse voltage TWs at the outlets of L_{21} and L_{23} can be obtained as follows:

$$\begin{cases} K_{SW1} = \dfrac{\left| \int \left(\Delta U_{dc2\_1} + \Delta I_{dc21} Z_{c\_L21} \right) \right|}{\left| \int \left(\Delta U_{dc2\_1} - \Delta I_{dc21} Z_{c\_L21} \right) \right|} \\ K_{SW2} = \dfrac{\left| \int \left(\Delta U_{dc2\_1} + \Delta I_{dc23} Z_{c\_L23} \right) \right|}{\left| \int \left(\Delta U_{dc2\_1} - \Delta I_{dc23} Z_{c\_L23} \right) \right|} \end{cases} \tag{8}$$

where ΔI_{dc21} and ΔI_{dc23} are the DC current variation at the outlets of L_{21} and L_{23}, respectively; and ΔU_{dc2_1} is the DC voltage variation at the DC bus in Fig. 1.

In addition, the time window should be selected within the range of $\left[t_0, t_0 + \min(2l_1/v, 2l_2/v)\right)$, where l_1 and l_2 are the lengths of L_{21} and L_{23}, respectively, and v denotes the propagation velocity of the TW.

III. Non-unit Protection Scheme Based on Cooperation with Control Strategy for the Multiterminal Hybrid HVDC System

For the multi-terminal hybrid HVDC system shown in Fig. 1, the DC line fault can be quickly and reliably detected based on the combination of the non-unit protection criterion and the direction criteria according to Section II. However, the configured protection cannot distinguish which line is the fault line. For example, for protection P_1 and P_3, fault f_1 and f_4 cannot be distinguished based on the local measured electrical quantities, because no DC inductor is installed on the DC line. Therefore, a non-unit protection scheme based on cooperation with control strategy is presented in this section, as shown in Fig. 4. The proposed strategy can realize fault isolation and system recovery based on local electrical information without line boundaries.

As shown in Fig. 4, for protection P_2, there is no DC line boundary element at either line outlet connected to station S_2, thus, the direction criterion independent of the line boundary can be utilized to identify the direction of the fault line. When protection P_2 is initialized by the starting criterion, the magnitude ratio of the forward and reverse TWs at the outlets of L_{21} (K_{SW1}) and L_{23} (K_{SW2}) can be calculated according to (8). Then, if $K_{SW1} \geqslant K_{s1}$ and $K_{SW2} \geqslant K_{s2}$, the fault can be judged as a reverse fault, indicating that no faults occur on either L_{21} or L_{23}. However, if $K_{SW1} < K_{s2}$, the fault can be judged as L_{21}-side DC fault, whereas if $K_{SW2} < K_{s2}$, the fault can be judged as a L_{23}-side DC fault. When the DC-line side fault is detected, whether the fault occurs on the DC line should be further determined by the protection criterion based on the transient voltage energy, as shown in (1) and (3).

However, for protection P_1 and P_3, it is difficult to identify the faults f_1 and f_4 based solely on the local measured electrical quantities, as no DC inductor is installed on the DC line. Taking protection P_1 as an example, non-unit protection based on cooperation with converter station control strategy is illustrated with one outgoing line (while the protection scheme of P_3 is similar). The detailed protection scheme is shown in Fig. 4.

When protection P_1 is started, the DC transient voltages at both sides of the DC inductor are calculated using the wavelet algorithm based on U_{dc1_1} and U_{dc1_s}. Therefore, the direction criterion based on the DC transient voltages at both sides of the DC inductor shown in (4) is utilized to identify the fault direction. A DC-line side fault can be detected when $K_{d1} > K_{s1}$, where K_{d1} is the magnitude ratio of the line side and converter side transient voltages of the DC inductor at protection P_1. When the fault is detected as a DC-line side fault, it is necessary to judge whether the fault occurs on the DC line by the transient-voltage-energy protection criterion. Thus, as shown in (1) and (2), if $E_{U1} > E_{s\_1}$, the fault can be judged to be on the DC line. Otherwise, the fault is a non-DC-line fault.

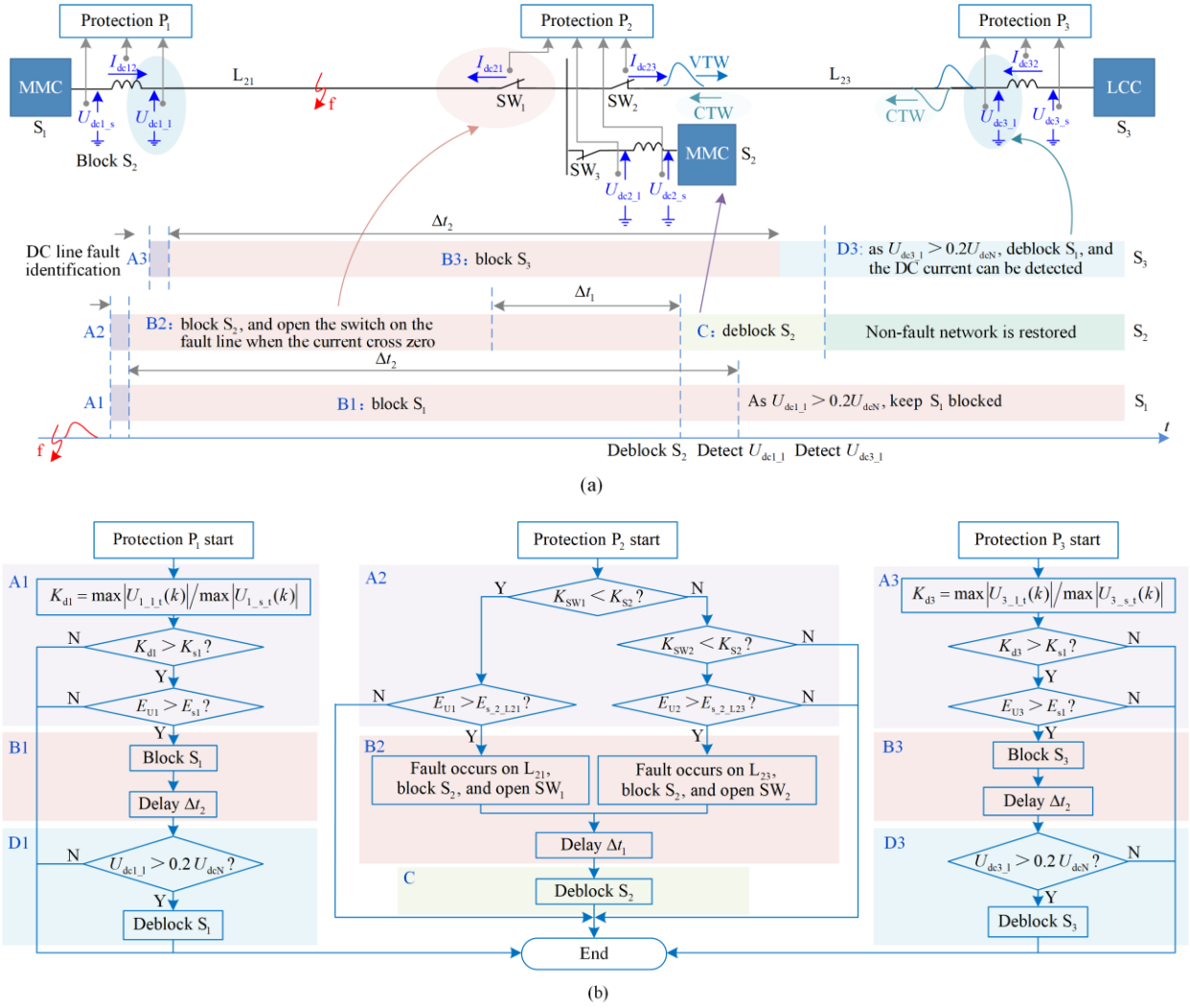

Fig. 4. The non-unit protection scheme based on cooperation with the control strategy. (a) The time sequence chart. (b) The protection process diagram.

Based on these constructs, if a DC-line fault is identified, the converter station should be blocked to suppress the DC current as soon as possible. When the converter station is blocked, the reverse polarity of the capacitor in the FBSM will be connected to the fault circuit, and the DC fault current can be quickly suppressed, and subsequently, the fault line can be isolated by the DC switches. After the opening of switches SW_1 or SW_2, converter station S_2 is deblocked following a delay period (Δt_1) to establish the DC voltage. Then, the voltage TW propagates along the line. In this case, for P_1 and P_3, the DC fault on L_{21} or L_{23} can be identified by checking whether the DC voltage is successfully

established. For example, for protection P_1, if there is no DC voltage after deblocking S_2 and a delaying period (Δt_2), this indicates that the fault is on L_{21}. In contrast, if the DC voltage satisfies $U_{dc1\_1} > 0.2U_{dcN}$ (U_{dcN} is the rated DC voltage) after deblocking S_2 and a delaying period of Δt_2, the fault can be identified as not occurring on L_{21}. In this situation, the non-fault network can be restored by deblocking converter station S_1. Otherwise, converter station S_1 remains blocked because the fault occurs on L_{21}. Specifically, Δt_2 is set to ensure that before converter station S_1 is deblocked, the fault line has been disconnected by the switch, and station S_2 is deblocked.

It should be noted that the basic principles of the protection criteria utilized in the proposed non-unit protection scheme are based on the fault-induced additional network. Therefore, the protection criteria rely on the fault components of voltage and current, which are obtained by subtracting the normal operation values from the sampling values. Consequently, the performance of the proposed protection method is not affected by the power flow direction of individual converter stations.

IV. Case Studies

A simulation model of the three-terminal hybrid HVDC grid shown in Fig. 1 is established to verify the feasibility of the proposed non-unit protection scheme based on cooperation with converter control. As shown in Fig. 1, inverter stations S_1 and S_2 are based on MMC, where the arm bridge is composed of HBSM and FBSM, while rectifier station S_3 is based on LCC. The main parameters of the system are listed in Table I. In addition, frequency-dependent overhead line model is utilized in the simulation model, and the detailed parameters of the HVDC lines are shown in Table II. Considering that the sampling rate of the protection equipment in HVDC projects is typically in the range of 10 kHz–20 kHz, the protection sampling rate is selected as 10 kHz in this paper. As analyzed in [19], the selected sampling rate meets not only the requirements of the protection criteria, but also the actual engineering requirements.

A. Applicability of Traditional Non-unit Protection

Non-unit protection is utilized as the main protection for the DC lines in an HVDC grid, and this approach can detect DC faults quickly, independent of line communication. Typical non-unit protection methods mainly rely on line boundaries, e.g., d*u*/d*t*-based protection, TW-based protection, and transient-component-based protection. Therefore, the operation performance of protection P_1 after positive pole-to-ground (PTG) faults f_1 and f_4 in Fig. 1 is shown to illustrate the applicability of traditional non-unit protection. The corresponding simulation results are shown in Fig. 5.

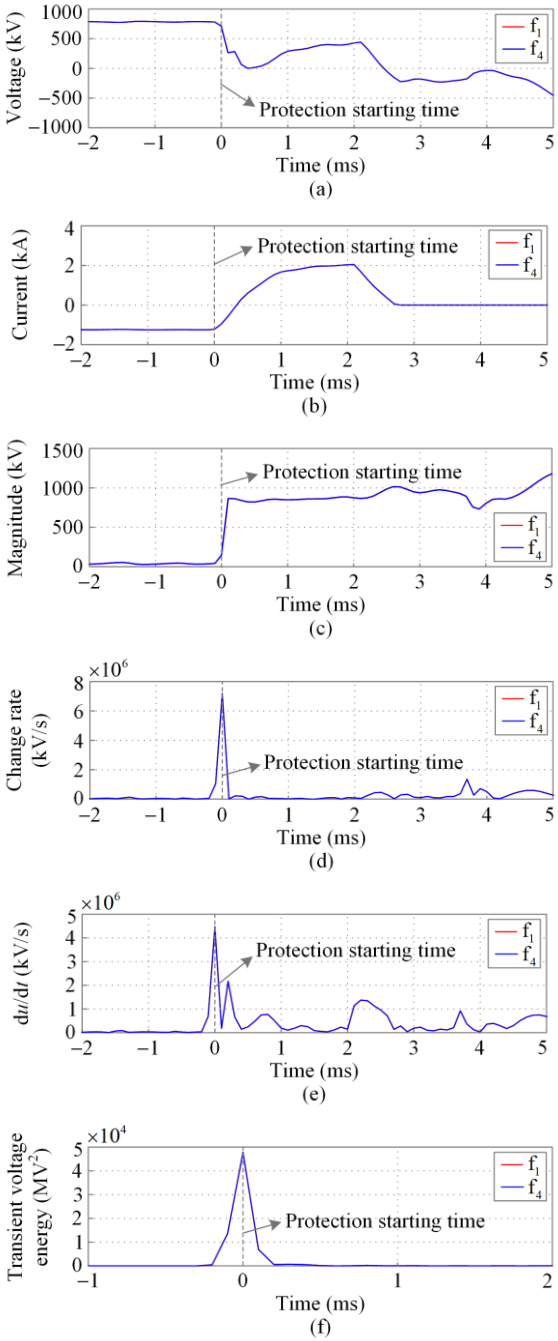

Fig. 5. Applicability of traditional non-unit protection for protection P_1. (a) The DC voltage. (b) The DC current. (c) Magnitude of the fault TWs. (d) Fault voltage TW change rate. (e) d*u*/d*t*. (f) Transient voltage energy.

For protection P_1, the electrical distance of fault f_1 equals to that of fault f_4 because no line boundary

exists between L_{21} and L_{23}. Thus, the DC electrical quantities after faults f_1 and f_4 are the same, resulting in the non-unit protection being unable to distinguish between the internal and external faults. The DC voltage and current after faults f_1 and f_4 are shown in Figs. 5(a) and (b), respectively. Consistent with the measured DC voltage and current, the magnitude and change rate of the fault voltage TW can be calculated, as shown in Figs. 5(c) and (d). When the magnitude or change rate of the fault TW is larger than the setting value of the protection criterion, the fault can be judged as an internal fault. However, faults f_1 and f_4 cannot be distinguished because the magnitude and change rate of the fault TWs for faults f_1 and f_4 are identical, as shown in Figs. 5(c) and (d). Similarly, the protection criteria based on the change rate of the voltage and transient voltage energy cannot distinguish between the internal fault f_1 and the external fault f_4, as shown in Fig. 5(e) and (f), respectively. In conclusion, non-unit protection based on line boundary cannot be applied to a multi-terminal hybrid HVDC grid, shown in Fig. 1.

B. Feasibility of the Non-unit Protection Scheme Based on Cooperation with the Control Strategy

The operations of converter stations S_1, S_2 and S_3 after faults f_1 and f_4 are observed to show the superiority of the proposed non-unit protection scheme based on cooperation with the control strategy over competing approaches. In this paper, the protection starting time is $t_0 = 0$, while Δt_1 and Δt_2 are selected as 30 ms and 100 ms, respectively. Based on [19] and [25], the time window of the protection criteria can be selected as $[t_0 - 1 \text{ ms}, t_0 + 2 \text{ ms}]$. It should be noted that, for the protection criteria based on the transient voltage, the db3 wavelet function with filter array length of six is utilized to extract the transient voltage. In order to eliminate the influence of the boundary effect, there need be at least four sampling points before the protection starting based on the basic principle of the wavelet algorithm [24]. When the time window is $[t_0 - 1 \text{ ms}, t_0 + 2 \text{ ms}]$ and the sampling rate is 10 kHz, the number of selected data window is 31, of which the number of the sampling data before the protection starting time is 10. Consequently, the selected time window can accurately reflect the fault, and the calculation results affected by the boundary should be discarded when identifying the fault.

In addition, for protection P_1 and P_3, the setting values of the protection criterion based on the DC transient voltage energy are 764 MV^2 and 1484 MV^2, respectively. For protection P_2, the setting value of the L_{21}-side protection criterion based on the DC transient voltage energy is 567 MV^2, and the setting value at the L_{23} side is 174 MV^2.

1) Fault Occurs on L_{21}

The simulation results for converter stations S_1, S_2, and S_3 when a metallic positive PTG fault occurs at the outlet of L_{21} are shown in Figs. 6–8, respectively.

For protection S_2, after fault f_1, the DC voltage drops, and the DC current rises rapidly. When protection P_2 is initialized, the fault direction is identified by the TW-based direction criterion. As shown in Fig. 6(a), the magnitude ratio of the forward and reverse TWs at the outlet of L_{21} is 0.34, which is less than the setting value of the protection criterion. However, the magnitude ratio at the outlet of L_{23} is 89.98, which is much larger than the setting value, as shown in Fig. 6(b). Therefore, the fault can be detected as a L_{21}-side fault based on the basic principle of the direction criterion. The DC transient voltage energy of protection P_2 calculated by the wavelet algorithm is shown in Fig. 6(c) to further determine whether the fault occurs on L_{21}. As shown in Fig. 6(c), the transient voltage energy in the selected time window of fault f_1 is $139\,930 \text{ MV}^2$, which is much larger than the setting value of 567 MV^2. Thus, the fault can be judged to occur on L_{21}. In this situation, converter station S_2 is blocked as soon as possible to suppress and clear the fault current, and the DC switch isolates the fault line when the DC current is small. After a delaying period of Δt_1, converter S_2 is deblocked at $t = 74$ ms, and the DC voltage is established, as shown in Fig. 6(d). Converter S_1 which is connected to the fault line cannot detect the DC voltage because the switch on the fault line is off, whereas converter S_3, which can detect the DC voltage, is deblocked quickly. The DC current can be detected on L_{23} after S_3 is deblocked as shown in Fig. 6(e), and the non-fault network is restored.

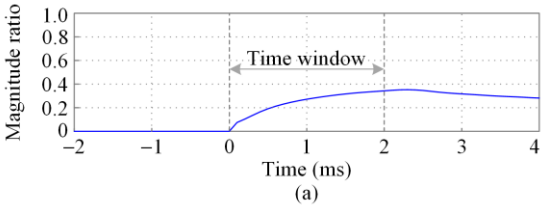

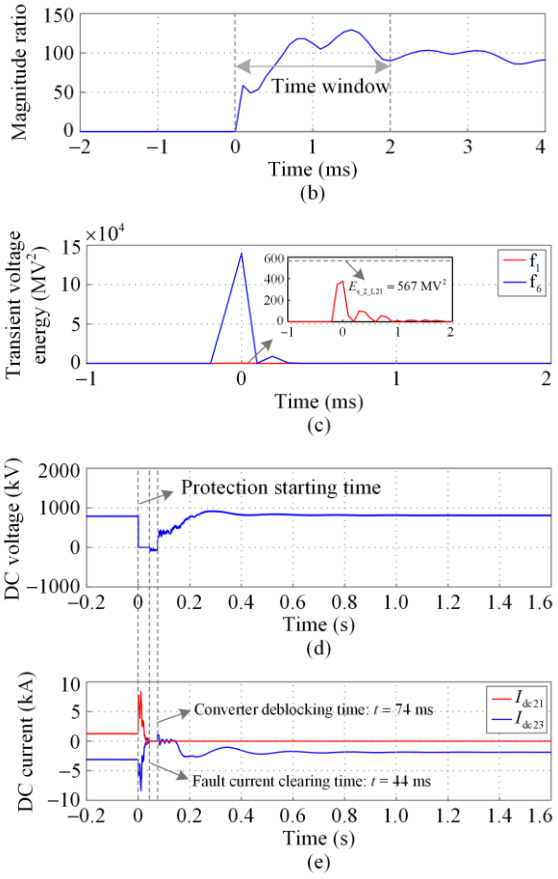

Fig. 6. Performance of protection P_2 and the operation of converter S_2 after fault f_1. (a) TW magnitude ratio of L_{21}. (b) TW magnitude ratio of L_{23}. (c) Transient voltage energy. (d) DC voltage at the outlet of the S_1. (e) DC current.

For protection P_1, protection can be started immediately when a fault occurs at the outlet of L_{21} resulting in rapid DC voltage drop and DC current rise. Direction protection based on the magnitude ratio of the line-side and converter-side transient voltages is utilized to judge the fault direction. According to the simulation results shown in Fig. 7, the transient voltage at the line side of the DC inductor is much larger than that at the converter side, and the magnitude ratio is calculated as 2.41, which is larger than the setting value 1.1. Therefore, the fault can be judged as a DC-line side fault. Subsequently, the line-side transient voltage energy of the DC inductor at the outlet of S_1 should be calculated to further determine whether the fault occurs on the DC line. As shown in Fig. 7(b), the DC transient voltage energy at the line side of the DC inductor after fault f_1 is 47 827 MV^2, which is much larger than the setting value of 764 MV^2. Thus, the fault can be judged to occur on the DC line. When the converter station is blocked and a delay time Δt_2 is elapsed, the DC fault can be identified by detecting the DC voltage. As shown in Fig. 7(c), a fault occurs on L_{21} which is connected to converter station S_1 as the DC voltage at the outlet of S_1 remains at zero. Therefore, converter station S_1 remains out of operation, and the DC current cannot be recovered, as shown in Fig. 7(d).

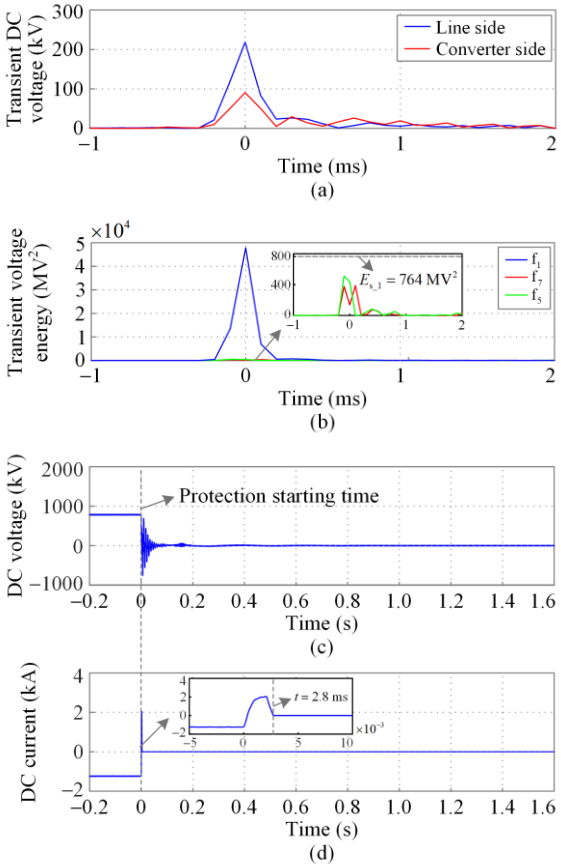

Fig. 7. Performance of protection P_1 and the operation of converter S_1 after fault f_1. (a) Transient DC voltage. (b) Transient voltage energy. (c) DC voltage. (d) DC current.

Similar to protection P_1, protection P_3 is started following the rapid drop of the voltage and rapid rise of the current after the DC fault. The fault can be judged to occur at the DC line side because the magnitude ratio of the line-side and converter-side transient voltages is 1.43, which is larger than the setting value, as shown in Fig. 8(a). The transient DC voltage energy is calculated to further determine whether the fault occurs on the DC line. According to the simulation results shown in Fig. 8(b), the maximum transient voltage energy after fault f_1 is 14 923 MV^2, which is much larger than the setting value of 1484 MV^2, and the fault can be judged to occur on the DC line. The DC voltage at the outlet of converter S_3 is shown in Fig. 8(c). When the converter is blocked, the DC voltage can be detected again after a delaying period of Δt_2. Therefore, the simulation results show that no fault occurs between converters S_2 and S_3, and

the non-faulting power system should be restored by deblocking converter S_3, as shown in Fig. 8(d).

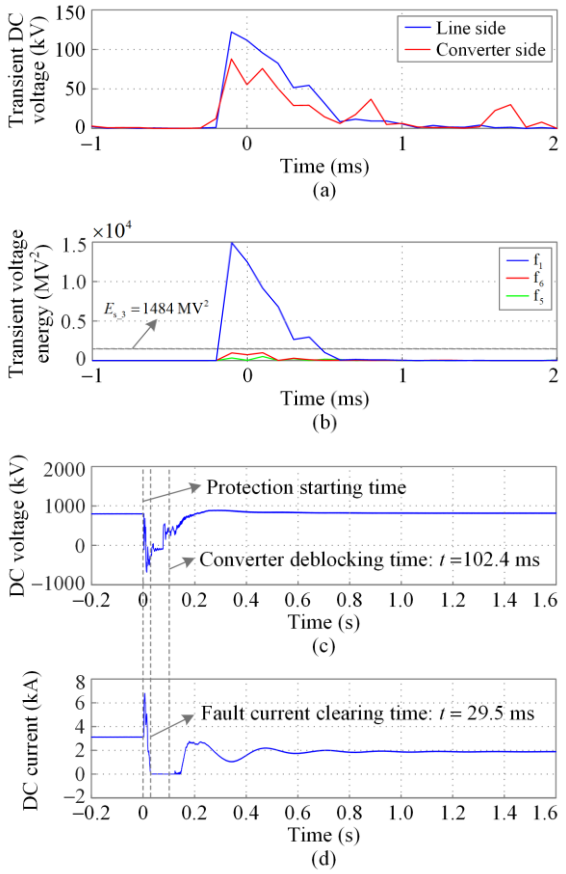

Fig. 8. Performance of protection P_3 and the operation of converter S_3 after fault f_1. (a) Transient DC voltage. (b) Transient voltage energy. (c) DC voltage. (d) DC current.

2) Fault Occurs on L_{23}

When a metallic positive PTG fault occurs at the outlet of L_{23}, the simulation results for converter stations S_1, S_2, and S_3 are shown in Figs. 9–11.

As shown in Figs. 9(a)–(b), the magnitude ratios of the forward and reverse TWs at the outlets of L_{21} and L_{23} are 110.20 and 0.30, respectively. Thus, the fault can be judged to occur on L_{23} by TW-based direction protection for protection P_2. Then, the transient DC voltage energy at the outlet of L_{23} is calculated as 139 900 MV^2, which is much larger than the setting value of 174 MV^2, as shown in Fig. 9(c). Therefore, the DC fault can be judged to occur on L_{23}. When the fault is judged as a DC-line fault, the converter should be blocked as soon as possible, and then switch SW_2 should be turned off once the DC fault current is small. After a delaying period of Δt_1, converter S_2 is deblocked to establish the DC voltage, as shown in Fig. 9(d). Considering that the fault line is isolated by SW_2, the DC voltage is not detected at the outlet of converter S_3, which is connected to the fault line. The current flows through L_{21} after deblocking converter S_1, as shown in Fig. 9(e), and the power system is restored.

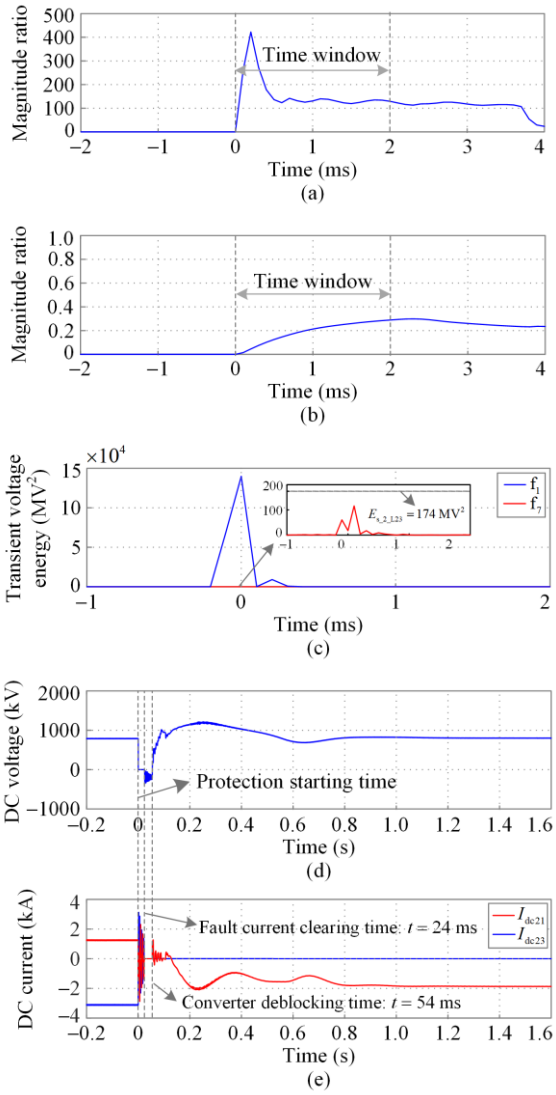

Fig. 9. Performance of the protection P_2 and the operation of converter S_2 after fault f_4. (a) TW magnitude ratio of L_{21}. (b) TW magnitude ratio of L_{23}. (c) Transient voltage energy. (d) DC voltage at the outlet of the S_1. (e) DC current.

The performance of protection P_1 is shown in Fig. 10. When it is started, the magnitude ratio of the line-side and converter-side DC transient voltages is calculated as 2.42, which is larger than the setting value of 1.1, as shown in Fig. 10(a). Thus, f_4 is judged as a forward fault for P_1. Subsequently, the transient voltage energy is calculated by using the wavelet transform algorithm to determine whether a fault occurs on the DC

line. In accordance with the simulation results shown in Fig. 10(b), the fault can be judged to occur on the DC line because the maximum magnitude of the transient voltage energy 47 806 MV^2 after fault f_4 is much larger than the setting value of 764 MV^2. Under these conditions, the converter should be blocked as soon as possible, while the voltage at the outlet of converter S_1 should be detected after a delaying period of Δt_2. The DC voltage at the outlet of S_1 is established again, indicating that no fault occurs between S_1 and S_2, as shown in Fig. 10(c). Therefore, converter S_1 is deblocked, and current flows through L_{21}, as shown in Fig. 10(d).

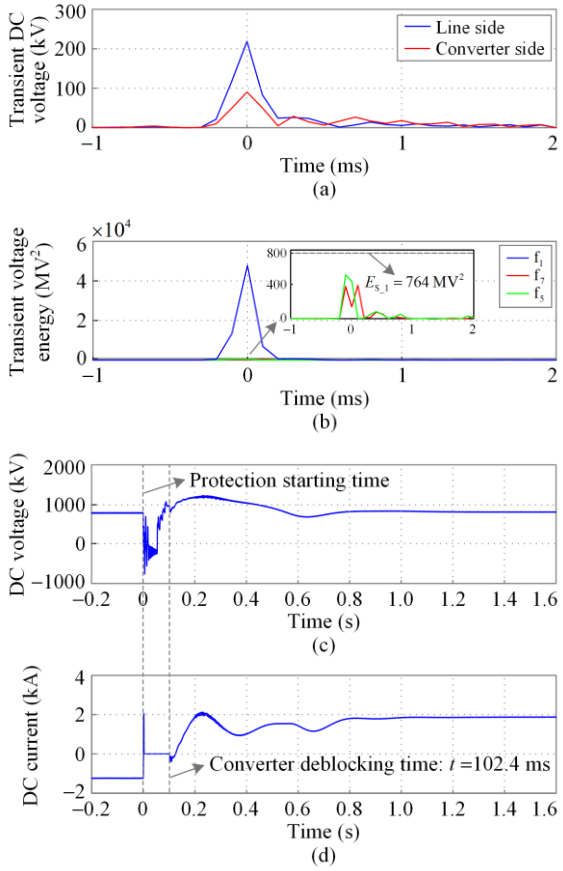

Fig. 10. Performance of the protection P_1 and the operation of converter S_1 after fault f_4. (a) Transient DC voltage. (b) Transient voltage energy. (c) DC voltage. (d) DC current.

Similar to protection P_1, protection P_3 identifies the fault direction first after start. The fault can be judged to be on the DC line side because the transient voltage magnitude ratio on both sides of the DC inductor (1.43) is larger than the setting value, as shown in Fig. 11(a). In Fig. 11(b), the maximum magnitude of the transient voltage energy after f_4 is 14 866 MV^2, which is much larger than the setting value of 1484 MV^2. Thus, the fault can be judged to be on the DC line. When a DC fault is identified, the converter should be blocked as soon as possible, and the voltage at the outlet of S_3 is shown in Fig. 11(c). In Fig. 11(c), the DC voltage is zero when the converter is blocked, even after a delaying period of Δt_2. This finding indicates that the fault occurred on L_{23}. Therefore, converter station S_3 remains blocked, as shown in Fig. 11(d).

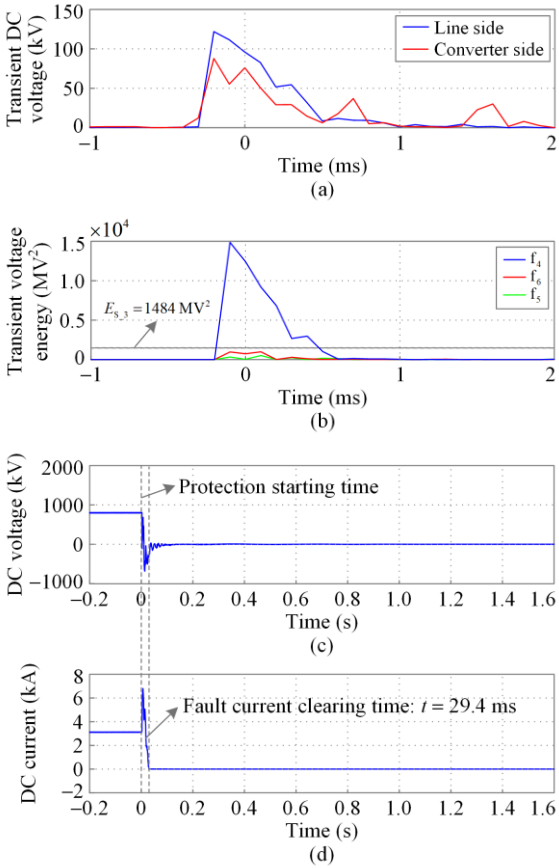

Fig. 11. Performance of protection P_3 and the operation of converter S_3 after fault f_4. (a) Transient DC voltage. (b) Transient voltage energy. (c) DC voltage. (d) DC current.

The simulation results indicate that the DC fault line can be reliably identified within 2 ms after the protection is started, while the converter can be blocked as soon as possible. Subsequently, the recovery of the non-fault network can be realized within a few hundred milliseconds after the fault.

C. Performances of the Non-unit Protection Scheme for Different Faults

1) Fault Transition Resistance Endurance

To verify the feasibility of the proposed non-unit protection scheme based on cooperation with the control strategy, various simulation tests are conducted, and the corresponding results are shown in Table III. The fault locations of $f_1 - f_9$ are shown in Fig. 1.

As shown in Table III, when the transition resistance is smaller than 300 Ω, for faults f_1, f_2 and f_8, which occur on L_{21}, protection P_1, P_2 and P_3 can judge the fault accurately, and after clearing the fault, converter stations S_2 and S_3 are restored. Similarly, for faults f_3, f_4 and f_9, the fault can be judged to occur on L_{23} by the proposed protection scheme, and converter stations S_1 and S_2 can be restored when the fault is cleared. In addition, for non-DC-line faults, such as f_5, f_6 and f_7, the fault can be reliably identified as external faults. This indicates that the proposed protection scheme has the ability to tolerate transition resistance. Consequently, for a multi-terminal hybrid HVDC system without line boundaries, the proposed non-unit protection scheme based on cooperation with the control strategy can detect and isolate faults reliably based on local electrical information, which can greatly accelerate the protection speed. The rapid recovery of the non-fault network can be realized, thereby greatly improving the power supply reliability.

TABLE III
PERFORMANCES OF THE NON-UNIT PROTECTION SCHEME FOR DIFFERENT FAULTS

Location	Transition resistance (Ω)	P_1		P_2			P_3		Correct operation?	Restored converter
		K_d	E_U (MV^2)	K_{SW1}	K_{SW2}	E_U (MV^2)	K_d	E_U (MV^2)		
f_1	0	2.41	47 827	0.34	89.98	139 930	1.43	14 923	√	S_2, S_3
	300	2.40	5027	0.34	28.39	15 099	1.17	1695	√	S_2, S_3
	500	2.38	2479	0.33	19.36	7219	1.03	857	Non-action	
f_2	0	2.24	138 890	0.35	84.33	11 102	1.96	11 102	√	S_2, S_3
	300	2.22	34 399	0.38	25.36	2545	1.63	6323	√	S_2, S_3
	500	2.22	19 277	0.38	16.91	1375	1.63	3482	√	S_2, S_3
f_3	0	2.38	30 890	105.27	0.31	3864	1.62	144 780	√	S_1, S_2
	300	2.42	7128	42.05	0.32	865	1.56	34 149	√	S_1, S_2
	500	2.37	4004	29.21	0.32	468	1.56	18 976	√	S_1, S_2
f_4	0	2.42	47 806	110.20	0.30	139 900	1.43	14 866	√	S_1, S_2
	300	2.45	5129	38.03	0.31	15 139	1.17	1678	√	S_1, S_2
	500	2.34	2481	25.83	0.31	7247	1.03	844	Non-action	
f_5	0	2.10	509	82.83	68.01	1376	Not start	514	√	
f_6	0	0.18	4696	0.36	51.07	378	1.65	989	√	
f_7	0	2.31	389	89.70	0.28	116	0.07	1167	√	
f_8	0	2.17	25 794	0.35	83.12	5964	1.48	32 680	√	S_2, S_3
	300	2.13	3155	0.34	32.47	750	1.49	3984	√	S_2, S_3
	500	2.07	1529	0.33	22.96	384	1.19	1949	√	S_2, S_3
f_9	0	2.40	17 053	86.95	0.32	9206	1.49	34 004	√	S_1, S_2
	300	2.40	1816	33.31	0.31	1027	1.81	3614	√	S_1, S_2
	500	2.39	875	23.06	0.30	498	1.78	1732	√	S_1, S_2

In addition, it should be noted that when the transition resistance increases to 500 Ω, there is a possibility of the protection maloperation. For example, when fault f_1 with 500 Ω occurs, protection P_3 cannot operate sensitively, as the transient voltage energy is smaller than the setting value.

2) Robustness Ability Against the Noise

The performances of protection P_2 after f_1 are taken as an example to evaluate the robustness against the noise. The white noise with a signal to noise ratio of 20 dB is added to the measured DC voltage and current, as shown in Figs. 12(a) and (b), respectively. For the DC voltage and current with the noise, the magnitude ratio of the forward and reverse TWs at the outlet of L_{21} is calculated as 0.36, while the value at the outlet of L_{23} is 12.57, as shown in Figs. 12(c) and (d). Thus, the fault can be judged to be at L_{21}-side. Then, the DC transient voltage energy can be obtained by the wavelet transform, as shown in Fig. 12(e). The maximum transient voltage energy in the selected time window of fault f_1 is 164 860 MV^2, which is much larger than the setting value, and thus, the fault can be judged to occur on L_{21}. Therefore, the proposed non-unit protection scheme is proved to be robust to noise.

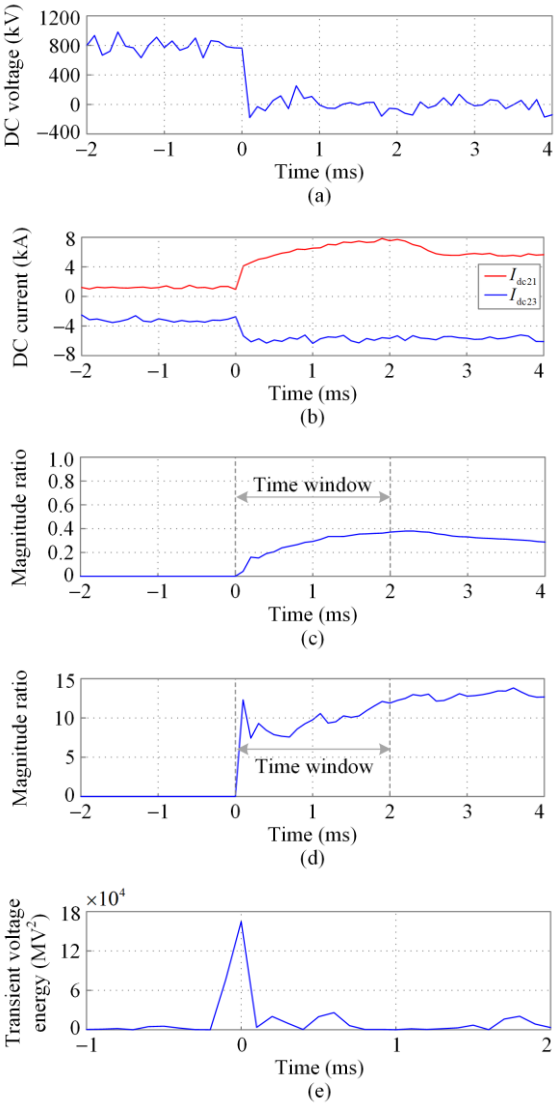

Fig. 12. The robustness ability against the noise for the protection P_2 after fault f_1. (a) DC voltage. (b) DC current. (c) TW magnitude ratio of L_{21}. (d) TW magnitude ratio of L_{23}. (e) Transient voltage energy.

V. Conclusion

Fast and reliable identification and isolation of DC faults are highly important for the safe and stable operation of multiterminal hybrid HVDC systems. However, existing non-unit protection schemes based on line boundary are not applicable in the case of multiterminal HVDC systems without line boundaries. Therefore, a non-unit protection scheme based on cooperation with the converter control strategy is proposed in this paper.

In the proposed DC protection scheme, the DC inductor at the outlet of the converter is utilized as the boundary for DC line faults and converter faults. The performances of the non-unit fault identification criteria and direction criteria are compared. In case only one outgoing line is connected to the converter station, DC faults can be identified directly by the criterion based on the transient voltage energy and the direction criterion based on the transient voltage magnitude ratio. For cases where several outgoing lines are connected to the converter station, DC faults are identified by the criterion based on the transient voltage energy and direction criterion based on the traveling wave. Therefore, DC line faults can be reliably identified by the proper setting value of the protection criterion, and selected converters can be blocked as soon as possible.

However, the configured protection cannot distinguish which line is the fault line. Thus, the cooperation control of individual converter stations is required to selectively identify the fault line. For converter stations connected with multiple DC lines, the fault line can be isolated by relevant DC switch, allowing the converter station to be deblocked to establish DC voltage. The deblocking of other converter stations is determined by the detection of the DC voltage, as only converter stations connected to non-fault lines can detect DC voltage.

In conclusion, the proposed non-unit protection scheme based on cooperation with the control strategy significantly improves the operation speed without the need for communication when compared to pilot protection. Unlike traditional non-unit protection schemes, this approach does not rely on line boundaries. The proposed protection scheme considers the operation speed, reliability, and sensitivity of protection while realizing fast recovery of non-fault network, thereby greatly improving the power supply reliability. In addition, for multiterminal HVDC grids based on the converters with fault clearing capability, the proposed non-unit protection scheme based on cooperation with converter control can be applied effectively.

Acknowledgment

Not applicable.

Authors' Contributions

Ye Li: writing-revised draft preparation and supervision. Na Jia: investigation and writing-review & editing. Jiawei He and Bin Li: methodology and visualization. Haiyang Wang: conceptualization. Shengbo Zhang: data curation and validation. All authors read and approved the final manuscript.

Funding

This work is supported by the National Natural Science Foundation of China (No. 52207088) and the Natural Science Foundation of Hebei Province (No. E2024202184).

Availability of Data and Materials

Not applicable.

DECLARATIONS

Competing interests: The authors declare that they have no known competing financial interests or personal relationships that could have appeared to influence the work reported in this paper.

AUTHORS' INFORMATION

Ye Li received the B.Sc., M.Sc., and Ph.D. degrees in electrical engineering from Tianjin University, Tianjin, China, in 2015, 2017, and 2021, respectively. Now she is serving as an associate professor in Hebei University of Technology, Tianjin, China. Her research field is involved in protection and fault ride-through control of flexible DC grid, protection and control of new power system with large-scale new energy access and so on.

Na Jia received a Bachelor's degree in electrical engineering and automation engineering from Shanxi University in Taiyuan, China in 2022. She is currently pursuing a Master's degree in electrical engineering at the School of Electrical Engineering, Hebei University of Technology, Tianjin, China. Her research interests include protection and control of flexible DC power grids.

Jiawei He received the B.Sc., M.Sc., and Ph.D. degrees in electrical engineering from Tianjin University, Tianjin, China, in 2014, 2017, and 2021, respectively. He is currently an associate researcher fellow with the School of Electrical and Information Engineering, Tianjin University. His research fields include protection and control of flexible dc grid, protection and control of power system with high proportion of renewable power generation, etc.

Bin Li received the B.Sc., M.Sc., and Ph.D.degrees in electrical engineering from Tianjin University, Tianjin, China, in 1999, 2002, and 2005, respectively. He was an academic visitor with The University of Manchester, Manchester, UK, in 2006. From 2008 to 2009, he worked in the design and application of protection relays with AREVA Company UK. He is currently a professor with the School of Electrical and Information Engineering, Tianjin University. His main research field includes the protection and control of power system.

Haiyang Wang is currently pursuing a Master's degree in electrical engineering at the School of Electrical Engineering, Hebei University of Technology, Tianjin, China. His research interests include renewable energy DC off-grid hydrogen production.

Shengbo Zhang is currently pursuing a Master's degree in electrical engineering at the School of Electrical Engineering, Hebei University of Technology, Tianjin, China. His research interests include protection and control of flexible DC power grids.

REFERENCES

[1] M. Zhou, J. Zhai, and G. Li *et al*., "Distributed dispatch approach for bulk AC/DC hybrid systems with high wind power penetration," *IEEE Transactions on Power Systems*, vol. 33, no. 3, pp. 3325-3336, May 2018.

[2] S. Zhang, M. Zhou, and Z. Liu *et al*., "Hierarchical flexible operation approach on a VSC-MTDC interconnected hybrid grid with a high share of renewable power," *IEEE Transactions on Power Systems*, vol. 37, no. 6, pp. 4936-4949, Nov. 2022.

[3] Y. Xue, Z. Xu, and G. Tang, "Self-start control with grouping sequentially precharge for the C-MMC-based HVDC system," *IEEE Transactions on Power Delivery*, vol. 29, no. 1, pp. 187-198, Mar. 2014.

[4] J. He, K. Chen, and M. Li *et al*., "Review of protection and fault handling for a flexible DC grid," *Protection and Control of Modern Power Systems*, vol. 5, no. 2, pp. 1-15, Apr. 2020.

[5] G. B. Oriol, S. B. Joan, and P. A. Eduardo *et al*., "Flexible converters for meshed HVDC grids: from flexible AC transmission systems (FACTS) to flexible DC grids," *IEEE Transactions on Power Delivery*, vol. 35, no. 1, pp. 2-15, Feb. 2020.

[6] H. Shu, S. Wang, and S. Lei, "Single-ended protection method for hybrid HVDC transmission line based on transient voltage characteristic frequency band," *Protection and Control of Modern Power Systems*, vol. 8, no. 2, pp. 1-11, Apr. 2023.

[7] N. M. Haleem, A. D. Rajapakse, and A. M. Gole *et al*., "Investigation of fault ride-through capability of hybrid VSC-LCC multiterminal HVDC transmission systems," *IEEE Transactions on Power Delivery*, vol. 34, no. 1, pp. 241-250, Feb. 2019.

[8] R. Zeng, L. Xu, and L. Yao *et al*., "Precharging and DC fault ride-through of hybrid MMC-based HVDC systems," *IEEE Transactions on Power Delivery*, vol. 30, no. 3, pp. 1298-1306, Jun. 2015.

[9] Y. Song, Y. Luo, and X. Xiong, "Loss distribution analysis and accurate calculation method for bulk-power MMC," *Protection and Control of Modern Power Systems*, vol. 8, no. 4, pp. 1-17, Oct. 2023.

[10] Y. Xiong, H. Rao, and S. Xu *et al*., "Research on start and fault ride-through strategy for ultra-high voltage multi-terminal hybrid DC transmission system," *Journal of Global Energy Interconnection*, vol. 1. no. 4, pp. 478-486, Sep. 2018.

[11] J. Zhang and C. Zhao, "The research of SM topology with DC fault tolerance in MMC-HVDC," *IEEE Transactions on Power Delivery*, vol. 30, no. 3, pp. 1561-1568, Jun. 2015.

[12] S. Li, J. Xu, and Y. Lu *et al*., "An auxiliary DC circuit breaker utilizing an augmented MMC," *IEEE Transactions on Power Delivery*, vol. 34, no. 2, pp. 561-571, Apr. 2019.

[13] Y. Shen, C. Huang, and Z. Zhao *et al*., "A traveling wave protection scheme for flexible DC power grids considering both short-circuit and breakage fault iden-

tification," *Power System Protection and Control*, vol. 52, no. 22, pp. 143-155, Nov. 2024. (in Chinese)

[14] J. Sneath and A. D. Rajapakse, "Fault detection and interruption in an earthed HVDC grid using ROCOV and hybrid DC breakers," *IEEE Transactions on Power Delivery*, vol. 31, no. 3, pp. 973-981, Jun. 2016.

[15] R. Li, L. Xu, and L. Yao, "DC fault detection and location in meshed multiterminal HVDC systems based on DC reactor voltage change rate," *IEEE Transactions on Power Delivery*, vol. 32, no. 3, pp. 1516-1524, Jun. 2017.

[16] W. Leterme, J. Beerten, and D. Van. Hertem, "Nonunit protection of HVDC grids with inductive DC cable termination," *IEEE Transactions on Power Delivery*, vol. 31, no. 2, pp. 820-828, Apr. 2016.

[17] W. Leterme and D. Van Hertem, "Cable protection in HVDC grids employing distributed sensors and proactive HVDC breakers" *IEEE Transactions on Power Delivery*, vol. 33, no. 4, pp. 1981-1990, Aug. 2018.

[18] J. Liu, N. Tai, and C. Fan, "Transient-voltage-based protection scheme for DC line faults in the multiterminal VSC-HVDC system," *IEEE Transactions on Power Delivery*, vol. 32, no. 3, pp. 1483-1494, Jun. 2017.

[19] B. Li, Y. Li, and J. He *et al*., "A novel single-ended transient-voltage-based protection strategy for flexible DC grid," *IEEE Transactions on Power Delivery*, vol. 34, no. 5, pp. 591-606, Oct. 2019.

[20] R. Zeng, L. Xu, and L. Yao *et al*., "Precharging and DC fault ride-through of hybrid MMC-based HVDC systems," *IEEE Transactions on Power Delivery*, vol. 30, no. 3, pp. 1298-1306, Jun. 2015.

[21] G. Song, J. Hou, and B. Guo *et al*., "Active injection for single-ended protection in DC grid using hybrid MMC," *IEEE Transactions on Power Delivery*, vol. 36, no. 3, pp. 1651-1662, Jun. 2021.

[22] F. Kong, Z. Gao, and S. Zhang *et al*., "Development of a novel protection device for bipolar HVDC transmission lines," *IEEE Transactions on Power Delivery*, vol. 29, no. 5, pp. 2270-2278, Oct. 2014.

[23] Z. Li, G. Zou, and B. Tong *et al*., "Novel traveling wave protection method for high voltage DC transmission line," in *2015 IEEE Power & Energy Society General Meeting*, Denver, USA, Jul. 2015, pp. 2980-2991.

[24] B. Li, Y. Li, and J. He *et al*., "An improved transient traveling-wave based direction criterion for the multi-terminal HVDC grid," *IEEE Transactions on Power Delivery*, vol. 35, no. 5, pp. 2517-2529, Oct. 2020.

[25] B. Li, Y. Li, and J. He *et al*., "Direction protection based on time-domain travelling wave for flexible MTDC grid," *CSEE Journal of Power and Energy Systems*, vol. 9, no. 4, pp. 1414-1424, Jul. 2023.

[26] J. He, Y. Sheng, and Y. Li, "A novel segmented-COV-based single-ended line protection algorithm for the multiterminal MMC-HVDC system with no boundary reactor," *IEEE Transactions on Industrial Informatics*, vol. 20, no. 4, pp. 5658-5670, Apr. 2024.

[27] Z. Bo, "A new non-communication protection technique for transmission lines," *IEEE Transactions on Power Delivery*, vol. 13, no. 4, pp. 1073-1078, Oct. 1998.

[28] Z. He, X. Wang, and Q. Qian. "A study of EHV transmission lines non-unit transient protection based on wavelet analysis," *Proceedings of the CSEE*, vol. 21, no. 10, pp. 10-14, 19, Oct. 2001. (in Chinese)

[29] C. Ma, B. Li, and J. He *et al*., "The improved fault location method for flexible direct current grid based on clustering and iterating algorithm," *IET Renewable Power Generation*, vol. 15, no. 15, pp. 3577-3587, Nov. 2021.